

Special Issue:

Special Issue on COVID-19 Aerosol
Drivers, Impacts and Mitigation

OPEN ACCESS 

Received: October 27, 2020
Revised: December 29, 2020
Accepted: December 30, 2020

* **Corresponding Author:**
yu.feng@okstate.edu

Publisher:
Taiwan Association for Aerosol
Research
ISSN: 1680-8584 print
ISSN: 2071-1409 online

 **Copyright:** The Author(s).
This is an open access article
distributed under the terms of the
[Creative Commons Attribution
License \(CC BY 4.0\)](https://creativecommons.org/licenses/by/4.0/), which permits
unrestricted use, distribution, and
reproduction in any medium,
provided the original author and
source are cited.

Assessing the Filtration Effectiveness of a Portable Ultraviolet Air Cleaner on Airborne SARS-CoV-2 Laden Droplets in a Patient Room: A Numerical Study

Yu Feng^{1*}, Jianan Zhao¹, Michele Spinolo², Kyle Lane², Darren Leung²,
Dave Marshall², Peter Mlinaric²

¹ School of Chemical Engineering, Oklahoma State University, OK 74078, USA

² CoV-Eng, 6 Queen Street, Leeds, West Yorkshire, LS12TW, UK

ABSTRACT

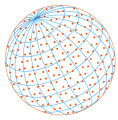
It has been confirmed that SARS-CoV-2 can infect humans via airborne transmission from person to person. Accordingly, there are two concerns about the exhaled airborne SARS-CoV-2 aerosol emitted from the coughs or sneezes of COVID-19 patients: (1) It might infect healthcare providers in the same confined patient rooms; (2) It might enter the main ventilation system and transmit to other patient room as a health threat. Therefore, a portable ultraviolet (UV) air cleaner is designed to mitigate the exposure risks to SARS-CoV-2 laden droplets in the patient room. Using the experimentally validated computational fluid-particle dynamics (CFPD) model, this study simulated the airborne transmission, deposition, and clearance of the COVID-19 virus-laden droplets emitted from a virtual patient in a virtual patient room with realistic ventilation conditions and various operating conditions of the portable UV air cleaner. Parameter analysis was performed to investigate how the ventilation conditions and the operation conditions of the sanitizer can influence the effectiveness of the filtration, which are quantified by the reduction of the concentration of virus-laden droplets suspended in the room and escaped from the room into the main ventilation system. Results indicate that the air cleaner is effective in virus-laden droplets clearance if placed in appropriate locations. In addition, maximizing the ventilation flow rate of the air cleaner will provide the best mitigation effect, with the highest filtration efficiency.

Keywords: COVID-19, Patient room; Portable UV air cleaner, Computational fluid-particle dynamics (CFPD), Cough droplets

1 INTRODUCTION

In the context of coronavirus disease 2019 (COVID-19), which is highly contagious and can spread among humans via airborne transmission, it is in urgent need for hospitals and other health care facilities to take care of COVID-19 patients. Since it has been confirmed by multiple research teams that SARS-CoV-2 RNA was found in the aerosol samples collected in COVID-19 patient rooms (Morawska *et al.*, 2020), infection controls for the airborne transmission of the SARS-CoV-2 in those patients room are crucial to minimizing the two potential health risks: (1) It might infect healthcare providers in the same confined patient room; (2) It might enter the main ventilation system and transmit to other patient rooms as a health threat.

According to the National Institute for Occupational Safety and Health (NIOSH) (NIOSH, 2015), the most effective way to control exposure to occupational hazards is the elimination, rather than social distancing and wearing personal protective equipment (PP). Thus, removing and reducing airborne SARS-CoV-2 is the most effective way to protect clinicians and other healthy healthcare workers who will be close to COVID-19 patients. According to such a priority, a novel designed



indoor portable ultraviolet (UV) air cleaner has been achieved (see Fig. 1). However, the optimized operation parameters and the filtration efficiency of the sanitizer in the patient room are not known yet, especially under the current ventilation conditions in the hospital.

Therefore, the objective of this study is to evaluate how the novel designed indoor UV air cleaner can positively affect the air quality by reducing the airborne COVID-19 virus-laden aerosol droplets emitted from a patient's cough. Employing a well-validated computational fluid-particle dynamics (CFPD) model (Feng *et al.*, 2020), this paper simulated the airborne transmission, deposition, and clearance of the COVID-19 virus-laden droplets emitted from a virtual patient in a virtual patient room with realistic ventilation conditions (Thatiparti *et al.*, 2016). Parameter analysis was performed to investigate how the ventilation conditions and the operation conditions of the sanitizer can influence the effectiveness of the filtration, which are quantified by the reduction of the concentration of virus-laden droplets suspended in the room and escaped from the room into the main ventilation system.

2 METHOD

2.1 Geometry and Computational Mesh

The proposed computational domain is shown in Fig. 1, including the patient room, main ventilation setup, patient bed, virtual patient, and the UV air cleaner. Specifically, the size of the patient room is 4.8 m (Length) \times 4.3 m (Width) \times 2.4 m (Height). The dimensions of the patient room are identical to the patient room documented in an existing paper (Thatiparti *et al.*, 2016). The virtual patient has a mouth opening with a hydraulic diameter equal to 20 mm. More details of the virtual patient geometry can be found in previous publications (Zhao *et al.*, 2019; Feng *et al.*, 2020). The UV air cleaner design, the portable UV air cleaner, uses ultraviolet (UV) light to kill the virus in a fully light sealed chamber (see Fig. 1), with 2 axial fans to suck the airborne virus-laden droplets in and generate clean air outflow from the bottom.

Mesh independence test has been performed by comparing the localized velocity magnitudes at 100 randomly selected locations in the patient room. Four polyhedron based meshes were generated with the average mesh element size refined by a factor of 3.375. The second most refined mesh was selected as the final mesh, which contains 9,427,248 elements, 33,834,226 nodes. Compared with the simulation results using the most refined mesh, the average relative velocity magnitude difference percentage is less than 5%.

2.2 Governing Equations

An Euler-Lagrange based multiphase flow method has been employed to track the cough

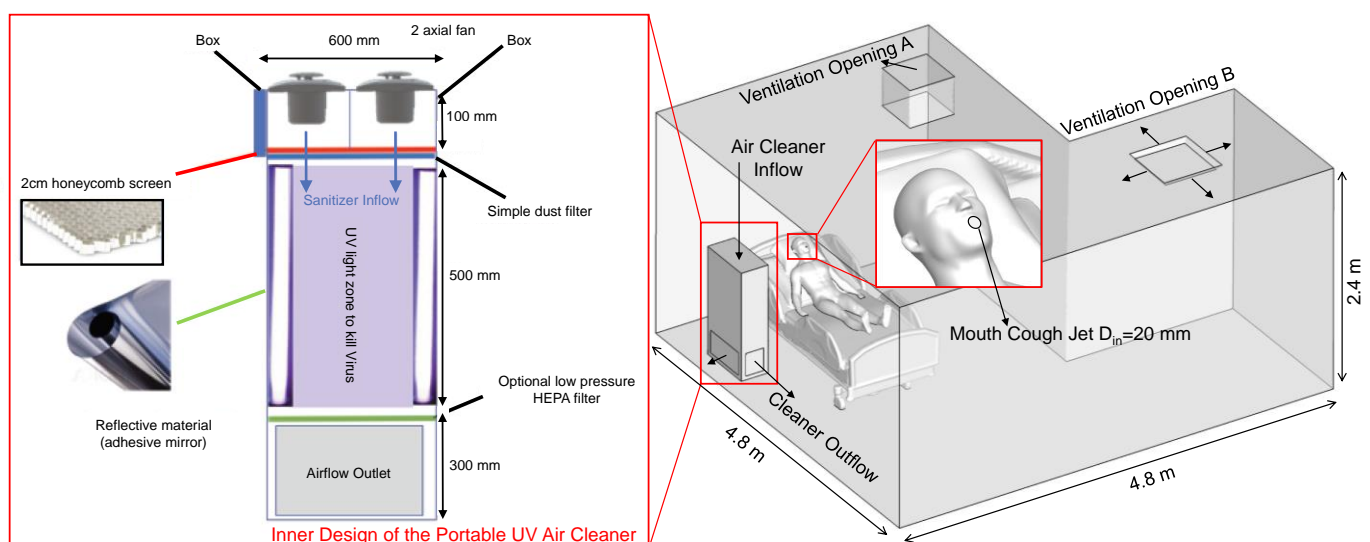
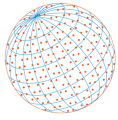


Fig. 1. Established design of the portable UV air cleaner, virtual patient room, patient bed, and the COVID-19 patient.



droplet size change simultaneously with their trajectories individually in the patient room due to the condensation/evaporation induced phase changes (Feng *et al.*, 2020). The governing equations can be found in (Chen *et al.*, 2017; Feng *et al.*, 2020).

2.3 Boundary Conditions

2.3.1 Transient cough jet waveform

A cough-jet airflow waveform based on the cough characterization data of 25 subjects (Yang *et al.*, 2018; Kuga *et al.*, 2020) is employed in this study (see Fig. 2(a)). Fourier series is used to generate the correlations of the transient airflow waveform applied as the boundary condition at the mouth opening of the coughing patient (see Fig. 1).

2.3.2 Initial size distribution of cough droplets

The widest span of the cough droplet size distribution measurements was used (Duguid, 1946) in this study (see Fig. 2(b)), which ranges from 2 to 2000 μm . The composition of the droplets is 10.4% NaCl and 89.6% water, which is used in previous studies (Haghnegahdar *et al.*, 2019; Feng *et al.*, 2020).

2.3.3 Main ventilation flow conditions

With the two ventilation openings at the ceiling (see Fig. 1), three main ventilation conditions were employed in this study to test the generality of the mitigation effectiveness using the portable UV air cleaner. As shown in Table 1, Cases A1–A3 use ventilation opening A as the exhaust and ventilation opening B as the airflow inlet, Cases B1–B3 use ventilation opening B as the exhaust and ventilation opening A as the airflow inlet, and Cases C1–C3 simulate the condition when the main ventilation is shut down. The main air exhaust $Q_{\text{main}} = 225$ CFM (382.27 m^3 per hour).

2.3.4 UV air cleaner flow rate and filtration conditions

Three UV air cleaner flow rates are employed in this study to quantify the effect of the operational condition of the UV air cleaner on filtration efficiency. The flow rates are $Q_{\text{as}} = 0$, 210 $\text{m}^3 \text{h}^{-1}$ (1X), and 1050 $\text{m}^3 \text{h}^{-1}$ (5X) (see Table 1). Cough droplets were assumed to be completely trapped when entering the UV air cleaner.

2.4 Numerical Setup

Numerical simulations were performed using ANSYS Fluent 2019 R1 (ANSYS Inc., Canonsburg,

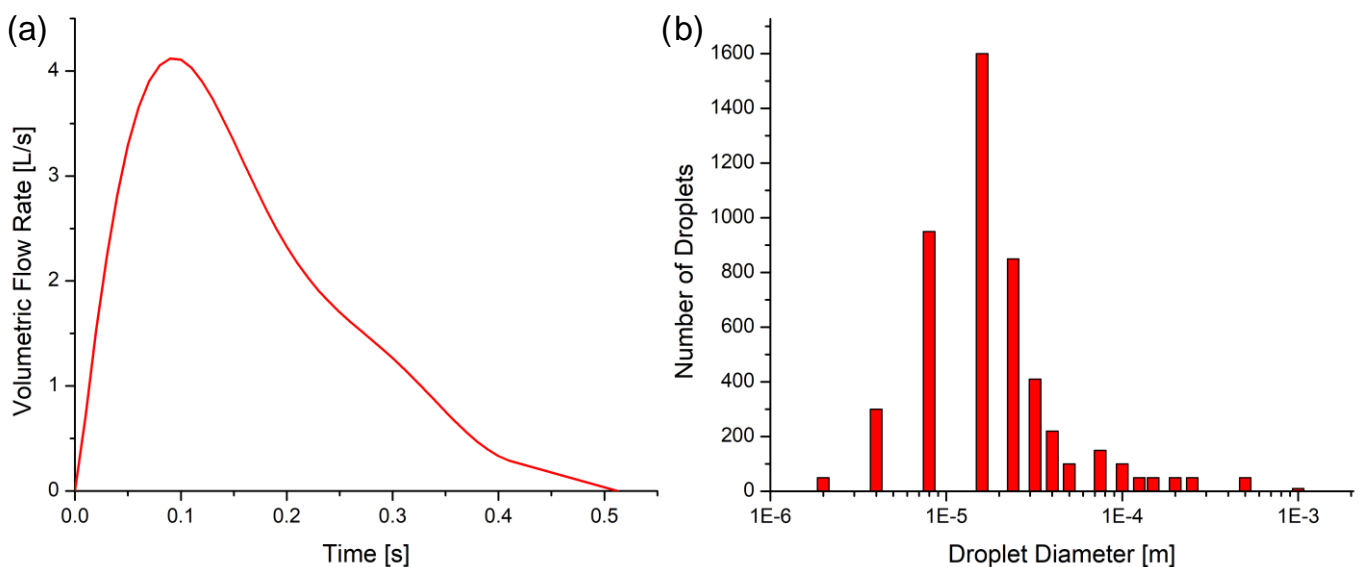
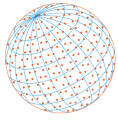


Fig. 2. Cough-jet boundary conditions at the mouth opening of the infected virtual human: (a) Transient cough-jet (reproduced from (Feng *et al.*, 2020)).

**Table 1.** Simulation case numbers associated with different ventilation conditions and UV air cleaner flow rates.

Case Number	UV Air Cleaner Status	UV Air Cleaner Flow Rate [m ³ h ⁻¹]	Ventilation Opening A	Ventilation Opening B
A1	Off	0 (0×)	Out	In
A2	On	210 (1×)	Out	In
A3	On	1050 (5×)	Out	In
B1	Off	0 (0×)	In	Out
B2	On	210 (1×)	In	Out
B3	On	1050 (5×)	In	Out
C1	Off	0 (0×)	0	0
C2	On	210 (1×)	0	0
C3	On	1050 (5×)	0	0

PA). Computational resources used include a local Dell Precision T7910 workstation (Intel®Xeon® Processor E5-2683 v4 with dual processors, 32 cores, and 256 GB RAM), and the supercomputer “Pete” at the High-Performance Computing Center (HPCC) at Oklahoma State University (OSU) (Intel®Xeon® Processor Gold 6130 CPU with dual processors, 32 cores, 64 threads, and 96 GB RAM). Convergence is defined for continuity, momentum, and supplementary equations when residuals are lower than 1.0e-4. The residuals for scalar transport equations are set as 1.0e-6 for convergence. Since a single cough releases within less than 0.55 s, a small time step $\Delta t_f = 0.005$ s was used when time $t < 0.6$ s, while $\Delta t_f = 0.01$ s when $t \geq 0.6$ s. The total physical time duration simulated is 100 s.

2.5 Model Validations

The credibility of the CFPD model has been extensively validated by the comparisons against benchmark experimental data on (1) laminar-to-turbulence airflow patterns, (2) droplet size change dynamics induced by condensation/evaporation, (3) particle depositions in complex computational domains. Details of the model validations can be found in previous publications (Feng *et al.*, 2017; Haghnegahdar *et al.*, 2018; Haghnegahdar *et al.*, 2019; Zhao *et al.*, 2019; Feng *et al.*, 2020).

3 RESULTS AND DISCUSSION

3.1 Airflow Fields in the Patient Room

Using the normalized velocity magnitude V^* , the quasi steady-state indoor airflow fields with different ventilation conditions and operational conditions of the UV air cleaner are visualized at selected planes in Figs. 3(a)–3(f). Specifically, V^* is defined as:

$$V^* = \frac{\|\vec{v}\|}{V_{\max}|_{Q_{AS} = 210 \text{ m}^3 \text{ h}^{-1}}} \quad (1)$$

where $V_{\max}|_{Q_{AS} = 210 \text{ m}^3 \text{ h}^{-1}}$ is the maximum velocity magnitude in the cases where $Q_{AS} = 210 \text{ m}^3 \text{ h}^{-1}$.

Airflow directions can be visualized via the velocity vector fields shown in Figs. 3(a)–3(f), while the recirculation characteristics can be observed from the streamlines. Specifically, with the same main ventilation conditions (see Cases A1 to A3 in Figs. 3(a)–3(c) as well as Cases B1 and B2 in Figs. 3(d) and 3(e)), increasing the UV air cleaner flow rate Q_{AS} will increase air circulations around the sanitizer. Specifically, with $Q_{AS} = 210 \text{ m}^3 \text{ h}^{-1}$ in Case A2 and Case B2, enhanced airflow at the top sanitizer inflow opening and the outflow openings near the floor can be observed in Figs. 3(b) and 3(e), compared with Cases A1 and B1 with the sanitizer shut down (see Figs. 3(a) and 3(d)). Compared with the air circular zones in Cases A1 and B1 shown by the streamlines and velocity vectors, more complex secondary flows and recirculation patterns can be found with the increase in Q_{AS} . With the further increase in Q_{AS} to $1050 \text{ m}^3 \text{ h}^{-1}$ (see Fig. 3(c) and Fig. 3(f) as two examples), double-vortex flow structures are generated on top of the sanitizer inflow opening. The double

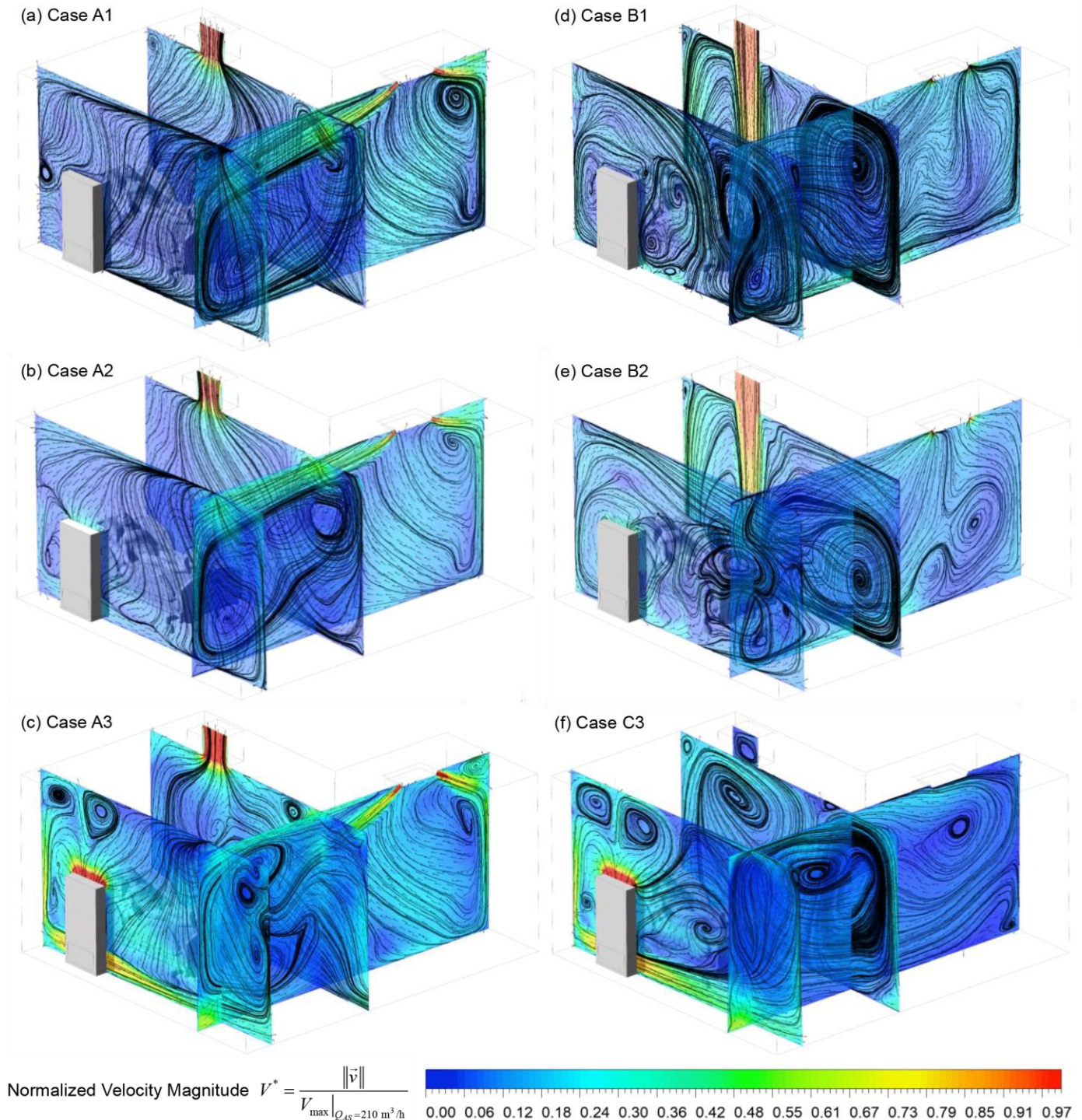
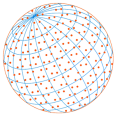
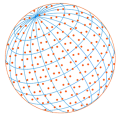


Fig. 3. Airflow fields in the patient room with different main ventilation conditions and operational conditions of the UV air cleaner: (a) Case A1, (b) Case A2, (c) Case A3, (d) Case B1, (e) Case B2, and (f) Case C3.

vortices are due to the combined effect of the stronger convection induced by the sanitizer inflow and the outflow, which are not influenced too much by the main ventilation conditions (see Figs. 3(c) and 3(f)). The double-vortex pattern is not observed when Q_{AS} is low (see Figs. 3(a), 3(b), 3(d), and 3(e)). The above-mentioned comparisons indicate that increase UV air cleaner flow rate Q_{AS} can potentially filter more cough droplets in a unit time. However, the enhanced convection and airflow recirculation may also carry small droplets further away from their generation sources and create a more scattered virus suspension pattern in the patient room. Figs. 3(a)–3(e)



also demonstrate that the main ventilation condition will also significantly alter the airflow patterns in the indoor room, which is dominant for the airflow field at locations not close to the UV air cleaner.

It is worth mentioning that the localized airflow patterns can significantly influence the cough droplet trajectories, especially for droplets with small aerodynamic diameters. The underlying connections between droplet transmission patterns and the airflow field characteristics are discussed in the following sections, associated with different ventilation and operational conditions.

3.2 Droplet Transmission and Deposition Patterns in the Patient Room

Transient droplet suspension patterns associated with different main ventilation conditions and UV air cleaner flow rates are shown in Figs. 4–7. It can be found that the droplet cloud shapes are not influenced significantly by the different main ventilation conditions or UV air cleaner flow rates at $t = 0.5$ s (see Figs. 4 (a), 5(a), 6(a), and 7(a)), which is close to the end of the cough. Indeed, during the cough, the initial momentum and energy of droplets obtained from the cough are still relatively high, so that the viscous dissipation effect given by the local airflows are negligible. However, the influence of the main ventilation and UV air cleaner flow rate becomes noticeable

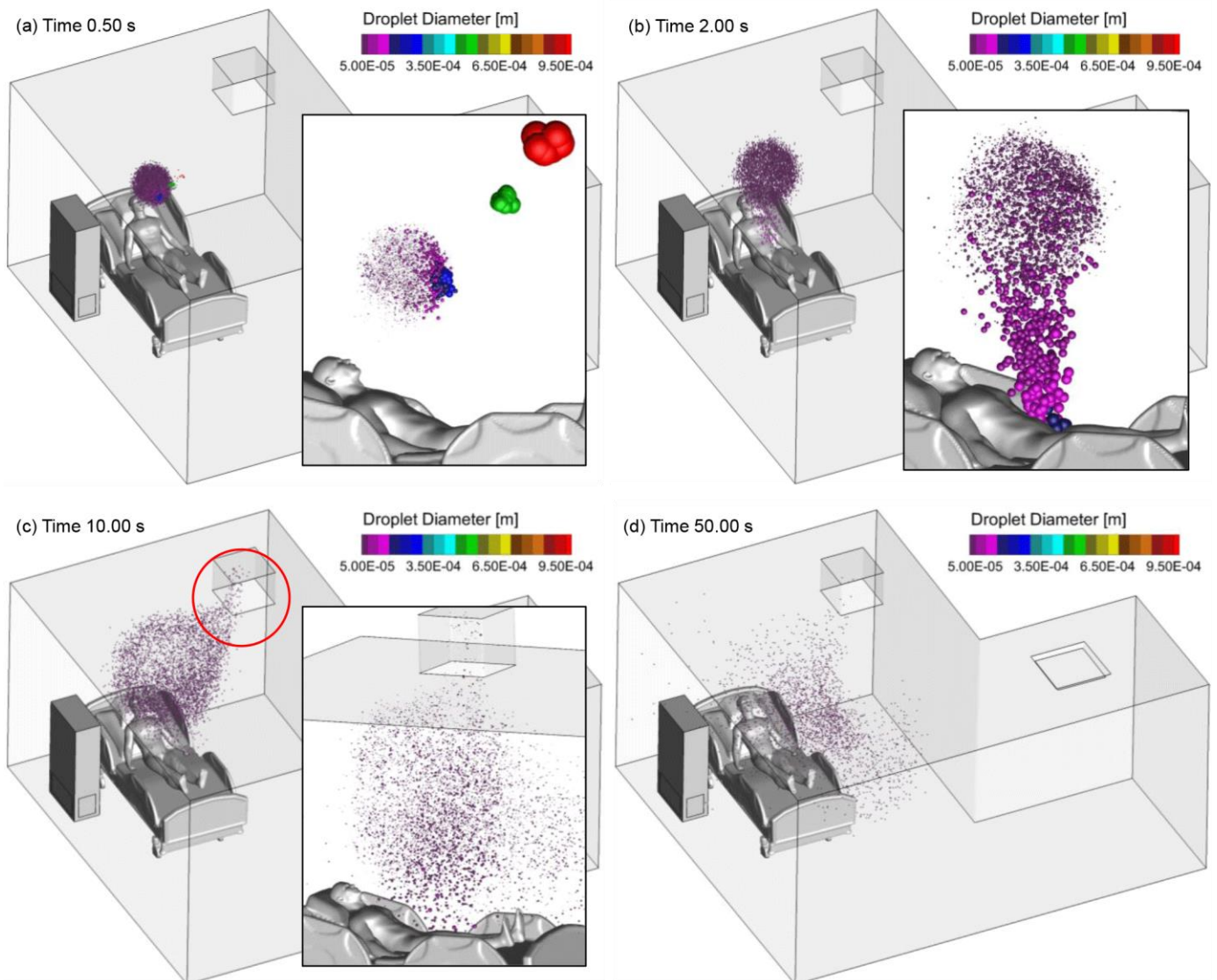


Fig. 4. Droplet suspension patterns at different time stations of Case A1 (sanitizer status: off $Q = 0 \text{ m}^3 \text{ h}^{-1}$): (a) $t = 0.5$ s, (b) $t = 2.0$ s, (c) $t = 10.0$ s, and (d) $t = 50.0$ s.

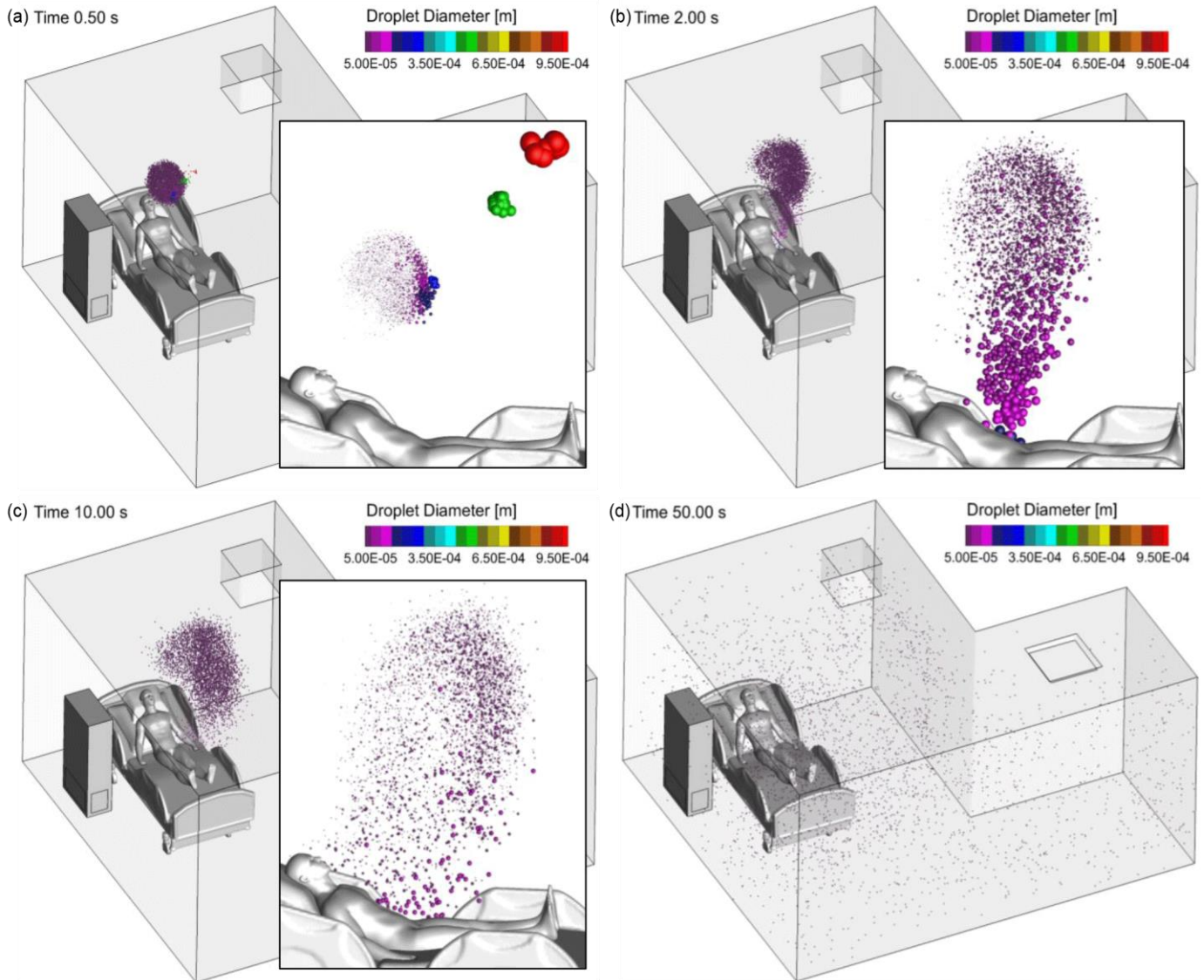
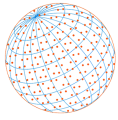


Fig. 5. Droplet suspension patterns at different time stations of Case B1 (sanitizer status: off $Q = 0 \text{ m}^3 \text{ h}^{-1}$): (a) $t = 0.5 \text{ s}$, (b) $t = 2.0 \text{ s}$, (c) $t = 10.0 \text{ s}$, and (d) $t = 50.0 \text{ s}$.

at $t = 2.0 \text{ s}$, 10.0 s , and 50.0 s . It can be also noticed that small droplets (colored purple) are more scattered in space, since their transport is influenced more by the airflow dispersion effect. In contrast, the trajectories of large droplets (colored blue, green, and red) are less influenced by the dispersion effect of the local airflow pattern, which is the reason that the locations of those droplets at different time stations are similar among cases with different main ventilation conditions and UV air cleaner flow rates.

Figs. 8(a)–8(f) visualize the deposition locations of SARS-CoV-2 droplets with different sizes, main ventilation conditions, and UV air cleaner flow rates. It can be observed that deposition locations of droplets with diameters larger than $200 \mu\text{m}$ are similar with different main ventilation conditions and UV air cleaner flow rates. Their transmissions are influenced dominantly by the gravitational sedimentation, negligibly by the airflow patterns. In contrast, deposition patterns of small droplets with diameters less than $20 \mu\text{m}$ are different among cases with different ventilation conditions and UV air cleaner flow rates. Specifically, deposition distributions are more scattered with main ventilation condition B (see Figs. 8(c) and 8(d)) compared with conditions A and C (see Figs. 8(a), 8(b), 8(e), and 8(f)). Such scattered deposition patterns are due to the convection direction of the main ventilation system, which is from the opening above the virtual patient head to the right opening. The main ventilation flow enhances the convection of the droplets from

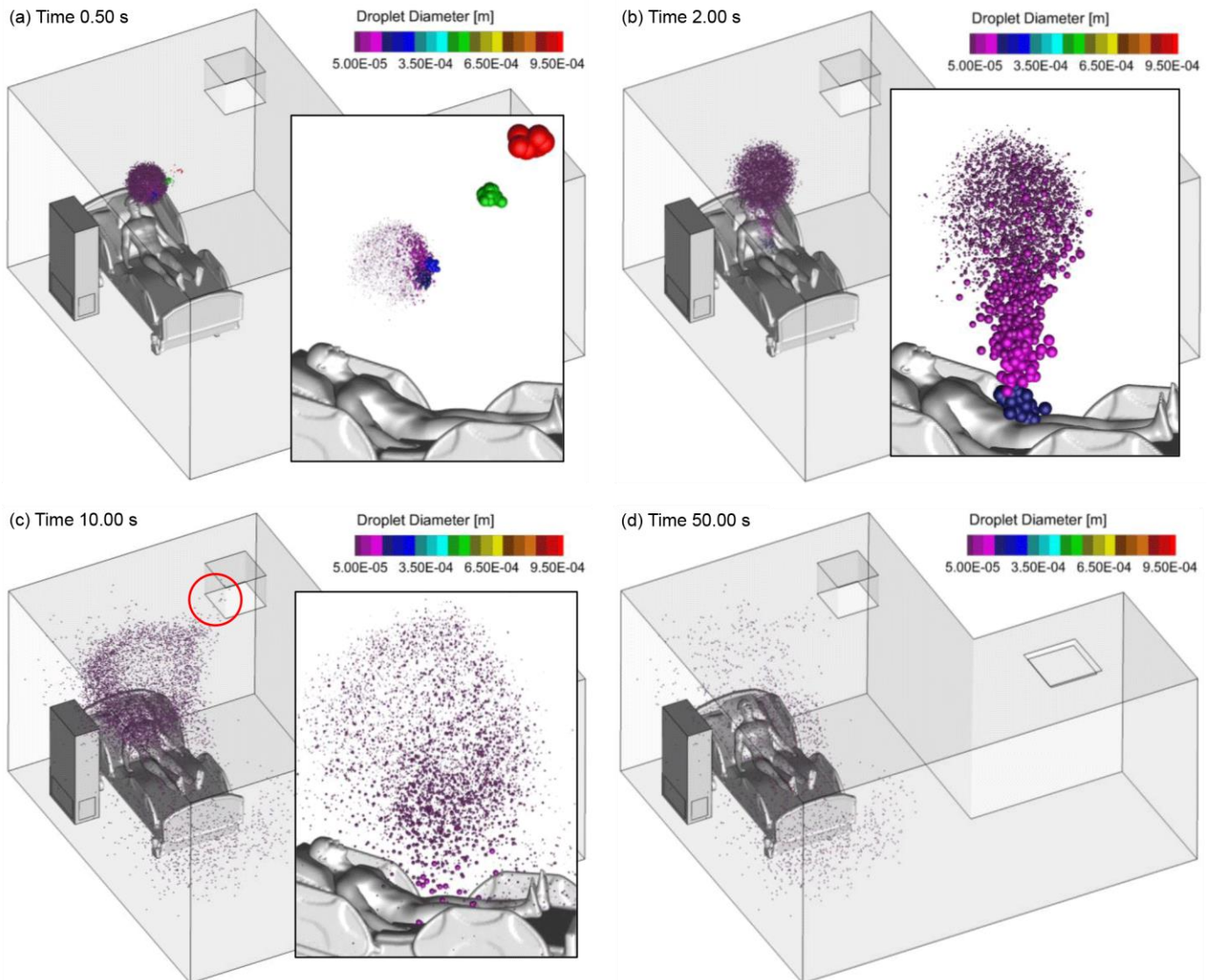
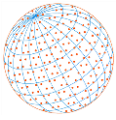


Fig. 6. Droplet suspension patterns at different time stations of Case A2 (sanitizer status: on $Q = 210 \text{ m}^3 \text{ h}^{-1}$): (a) $t = 0.5 \text{ s}$, (b) $t = 2.0 \text{ s}$, (c) $t = 10.0 \text{ s}$, and (d) $t = 50.0 \text{ s}$.

the patient bed to the right side of the room. In addition, increase $Q_{AS} = 0 \text{ m}^3 \text{ h}^{-1}$ (see Figs. 8(a), 8(c), and 8(e)) to $Q_{AS} = 1050 \text{ m}^3 \text{ h}^{-1}$ (see Figs. 8(b), 8(d), and 8(f)) will shift the droplet cloud deposited on the patient body towards the UV air cleaner, and reduce the number of droplets deposited in the patient room. Such observations are due to the enhanced filtration effect with the higher Q_{AS} . It is interesting to notice that the deposition on the floor downstream to the UV air cleaner in Fig. 8(f) is more intense than what is shown in Fig. 8(e). This is because the high outlet flow from the UV air cleaner in Case C3 can create flow circulation and bring more droplets from the cough to the floor than in Case C1 with the UV air cleaner shut down. In summary, depositions of small SARS-CoV-2 laden cough droplets can be controlled with the optimization of main ventilation conditions, UV air cleaner locations, and the UV air cleaner flow rate.

3.3 Main Ventilation Influence on Cough Droplet Transmission and Filtration

To investigate the main ventilation influence on droplet transmission and filtration, Figs. 4 and 5 visualize the airborne droplet transmissions in Case A1 and Case B1 with the UV air cleaner shut down. It can be found from Figs. 4(a)–4(d) that with the exhaust located near the patient bed, more droplets are carried by the suction flow into the main ventilation system (see the red circle in Fig. 4(c)), which may introduce potential exposure risks to other rooms. In contrast, with the

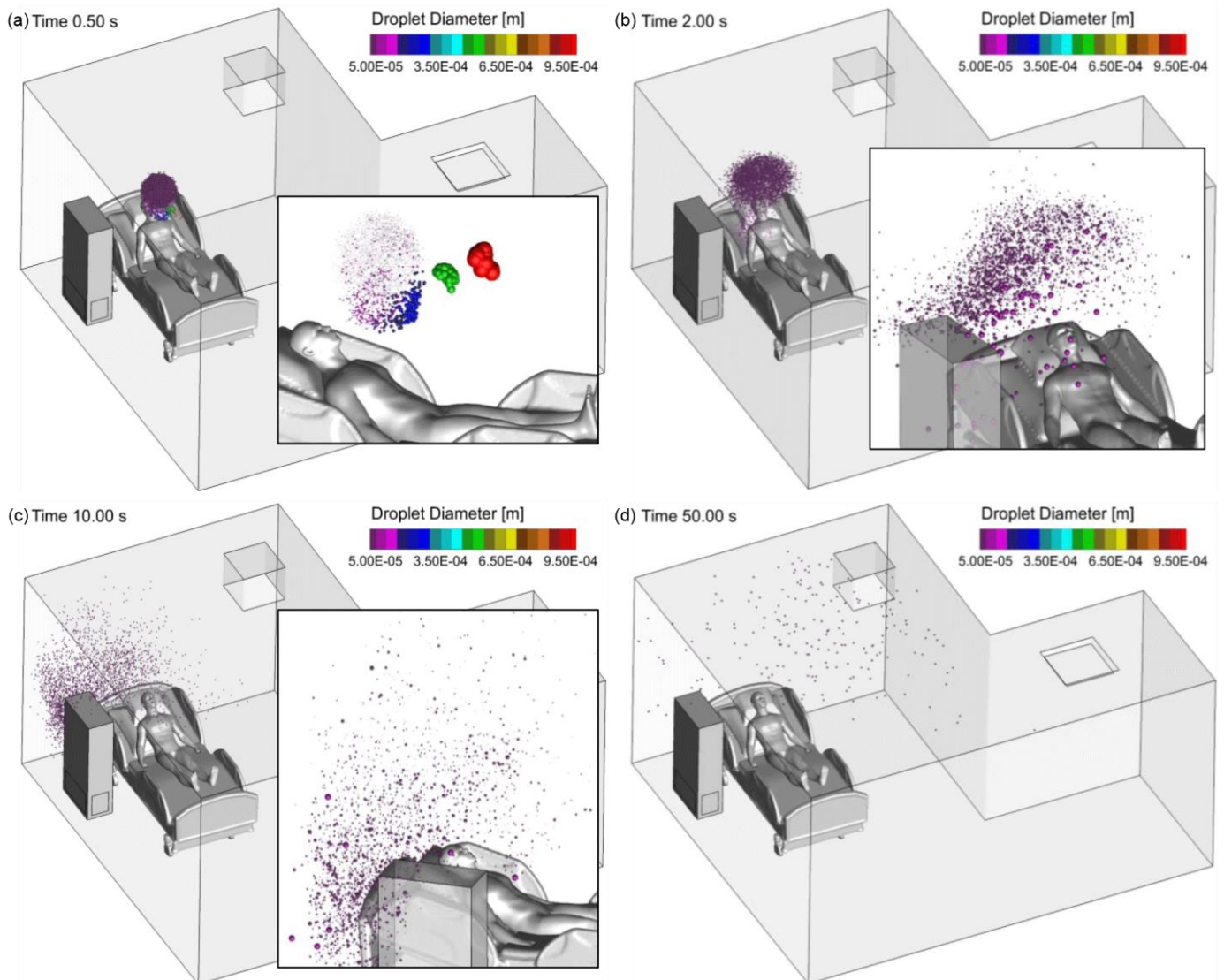
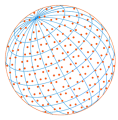


Fig. 7. Droplet suspension patterns at different time stations of Case A3 (sanitizer status: on $Q = 1050 \text{ m}^3 \text{ h}^{-1}$): (a) $t = 0.5 \text{ s}$, (b) $t = 2.0 \text{ s}$, (c) $t = 10.0 \text{ s}$, and (d) $t = 50.0 \text{ s}$.

inflow opening located on top of the patient bed (see Figs. 5(a)–5(d)), the droplet distributions are more scattered in the room (see Fig. 5(d)) than what is shown in Fig. 4(d). Integrating the observations provided in the previous section, it can be concluded that the main ventilation conditions have a noticeable influence on the transmission of small droplets, but a negligible influence on large droplets. Considering the longer residence time of the small droplets, the main ventilation system needs to be designed well to create preferable airflow distributions in the indoor environment to minimize the escaped droplet number through the exhaust and retain a smaller zone for droplet suspension. The same conclusions are to be also drawn based on the deposition patterns shown in Figs. 8(a)–8(f).

3.4 Influence of the UV air cleaner Flow Rate on Cough Droplet Transmission and Filtration

Using Cases A1 to A3 as an example to show the influence of the UV air cleaner flow rate on cough droplet transmission, Figs. 4, 6, and 7 visualize the droplet transmission pattern shifts associated with different Q_{AS} . It can be found that with the increase in Q_{AS} , the cough droplet cloud shifts faster to the UV air cleaner at $t = 2.0 \text{ s}$ and $t = 10.0 \text{ s}$. Also, increasing the suction power of the UV air cleaner avoids more droplets to be drawn into the main exhaust as shown

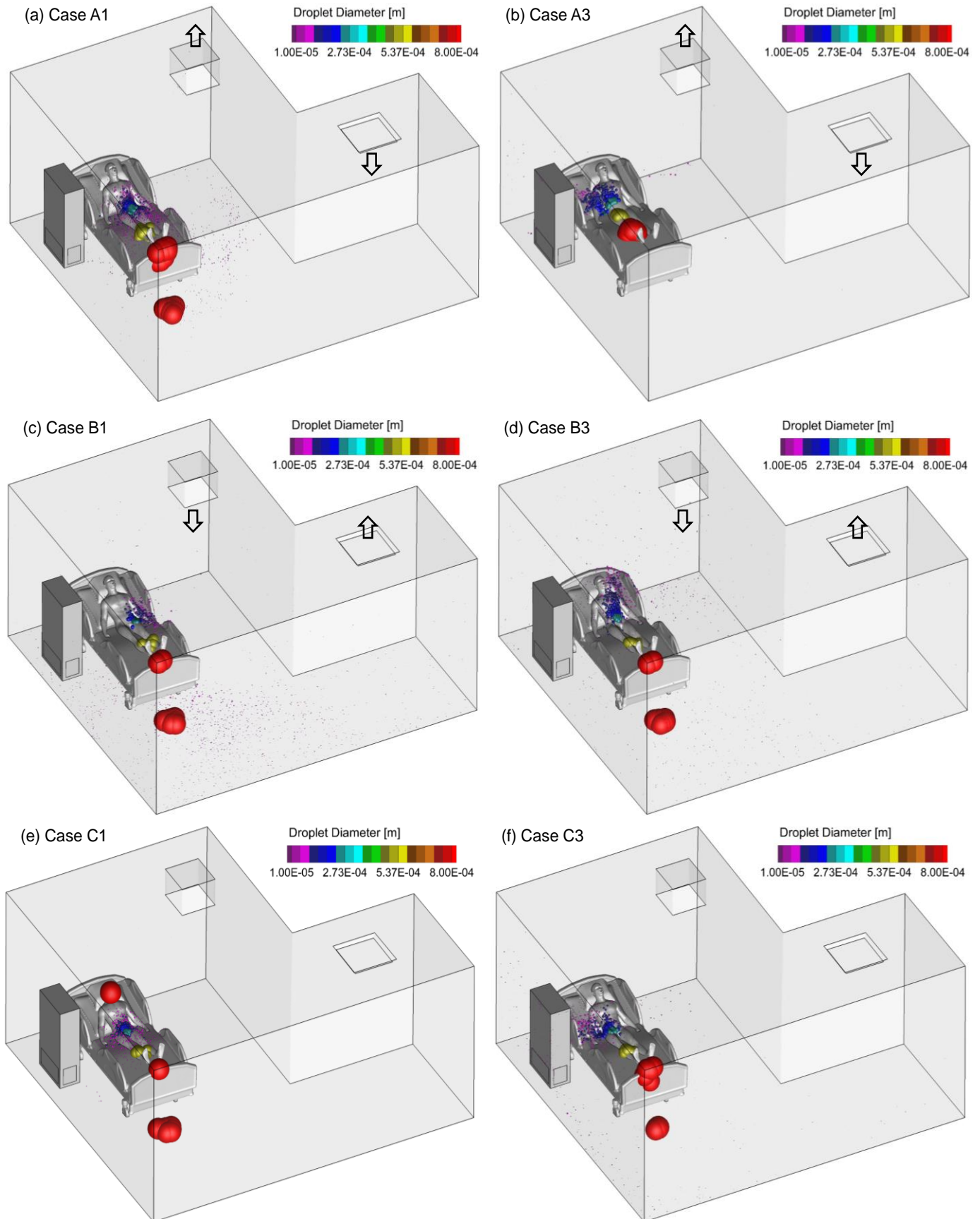
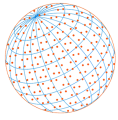
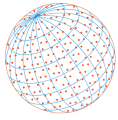


Fig. 8. Droplet deposition patterns with different ventilation conditions and operational conditions of the UV air cleaner: (a) Case A1, (b) Case A3, (c) Case B1, (d) Case B3, (e) Case C1, and (f) Case C3.



at $t = 10.0$ s. It can also be observed that higher Q_{AS} can remove the virus-laden droplets more effectively, supported by the droplet suspension pattern comparisons between Figs. 4(d), 6(d), and 7(d). The observation can also be supported by the deposition pattern comparisons shown in Figs. 8(a)–8(f). Figs. 8(a)–8(f) also indicate that the UV air cleaner is efficient to filter small droplets with diameters less than $10 \mu\text{m}$. Large droplets with diameters larger than $20 \mu\text{m}$ deposit before they can be drawn into the UV air cleaner. Increasing Q_{AS} further may improve the filtration effectiveness for larger droplets.

3.5 Evaluation of the Mitigation Effectiveness

Three variables need to be quantified as the direct indicators of the exposure risk and the effectiveness of the mitigation strategy using the UV air cleaner. The mitigation effectiveness is considered high if:

- (1) Droplets number fraction filtered by the UV air cleaner is high;
- (2) Droplets number fraction escaped into the main ventilation system is low; and
- (3) Droplets number suspended in the patient room is low.

Accordingly, three number fractions are defined as follows to facilitate the analysis of mitigation effectiveness, i.e.,

$$\eta_F = \frac{\text{Number of Droplets Filtered}}{\text{Number of Droplets Generated}} \quad (2)$$

$$\eta_E = \frac{\text{Number of Droplets Escaped from Main Exhaust}}{\text{Number of Droplets Generated}} \quad (3)$$

$$\eta_S = \frac{\text{Number of Droplets Suspending in the Room}}{\text{Number of Droplets Generated}} \quad (4)$$

where η_F is the UV air cleaner filtration efficiency, η_E is the escaped droplet number fraction, and η_S is the suspended droplet number fraction.

Figs. 9(a)–(c) show η_F , η_E , and η_S with different main ventilation conditions and UV air cleaner flow rates. As shown in Fig. 9(a), the filtration efficiency η_F is enhanced with the increase in UV air cleaner flow rate in all three main ventilation conditions (see Table 1 for the three main ventilation conditions employed in this study). The improvement in filtration efficiency is due to the increased droplet number flow rate entering the UV air cleaner induced by the stronger suction power. The underlying mechanisms can also be observed from the comparisons of droplet cloud locations and number concentrations in Figs. 4, 6, and 7 (Cases A1, A2, and A3). Specifically, with a higher UV air cleaner flow rate (see Case A3 in Fig. 7), more droplets traveled faster and entered the UV air cleaner, and fewer droplets suspended in the air compared with

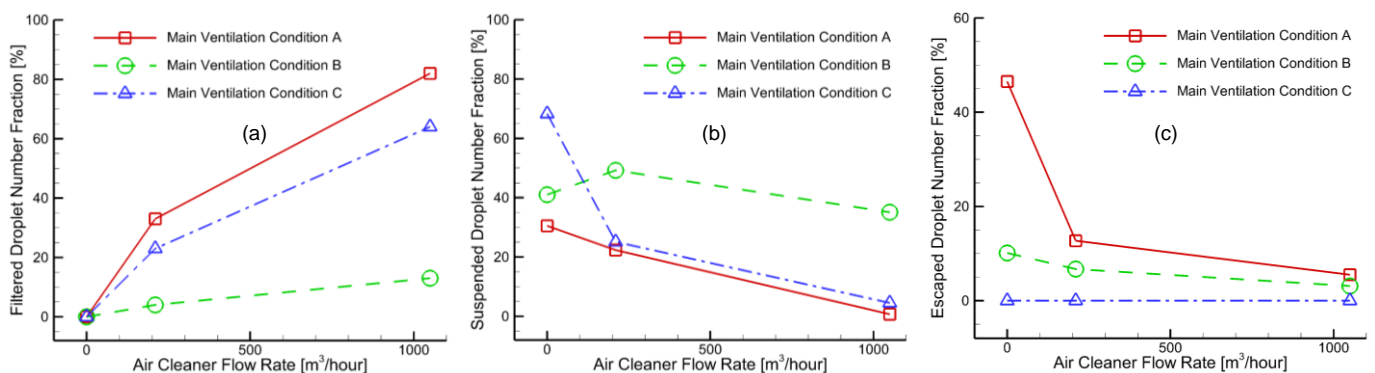
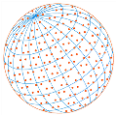


Fig. 9. Cough droplet fates with different main ventilation conditions and operational conditions of the UV air cleaner at $t = 100$ s: (a) filter droplet number fraction, (b) suspended droplet number fraction, and (c) escaped droplet number fraction from the main ventilation system.



cases with low UV air cleaner flow rates (see Case A1 and A2 in Figs. 4 and 6). However, the influence of the UV air cleaner flow rate on the suspended droplet number is dependent on the main ventilation conditions (see Fig. 9(b)). Specifically, increasing the UV air cleaner flow rate will decrease the concentration of the suspended droplets for main ventilation conditions A and C. In contrast, with main ventilation condition B, the suspended droplet number in Case B2 is higher than Case B1. Indeed, the enhanced convection caused by the UV air cleaner in Case B2 can increase the droplet suspension and distribution in the room, which is more dominant than the improved filtration effectiveness. In addition, with the main ventilation system on (Cases A1–A3 and Cases B1–B3), increasing the UV air cleaner flow rate will reduce the escaped droplet number fraction η_E into the main ventilation system (see Fig. 9(c)), indicating a reduced risk of the transmission of the virus from the patient room to other rooms via the ventilation system. Therefore, it can be concluded the highest UV air cleaner flow rate ($Q_{AS} = 1050 \text{ m}^3 \text{ h}^{-1}$ (5X)) can provide the optimized mitigation effectiveness by providing the highest filtration efficiency, lowers suspended and escaped droplet number fractions.

In addition, it can also be observed that the filtration efficiencies are the highest with main ventilation condition A than conditions B and C (see Fig. 9(a)). Specifically, η_F can be up to 82% approximately. This is because the exhaust in the main ventilation condition A is located above the patient bed, which creates airflow fields that can dissipate the momentum of the cough droplets that move away from the UV air cleaner (see Fig. 3(a)–3(c)). Because the exhaust in main ventilation condition A is the closest to the cough droplet generation site, the escaped droplet number fractions η_E are the highest in condition A compared with conditions B and C (see Fig. 9(c)). Thus, although main ventilation condition A can most effectively reduce the exposure risk in the patient room, it will also create the highest risk with the highest transmission capability of the virus-laden droplets into other rooms via the ventilation system.

In summary, the relative positions among the UV air cleaner, patient, and the main exhaust play a key role in the mitigation effectiveness of the exposure risks to airborne SARS-CoV-2 laden cough droplets.

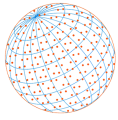
4 CONCLUSIONS

In this study, an experimentally validated CFPD model has been employed as a noninvasive assessment tool to quantify the exposure risk and the effectiveness of the mitigation strategy using a UV air cleaner in the patient room to the airborne SARS-CoV-2 laden droplets. The generation, transmission, deposition, and clearance of airborne SARS-CoV-2 laden droplets have been simulated and compared with different main ventilation conditions and UV air cleaner operational conditions in a COVID-19 positive patient room. Major conclusions are listed as follows:

- Transmission of cough droplets less than $20 \mu\text{m}$ in diameter are sensitive to the ventilation conditions and can be filtered by the UV air cleaner more effectively. In contrast, larger droplets will be dominated by the gravitational effect and will be insensitive to the ventilation conditions and UV air cleaner flow rate conditions.
- Although increasing UV air cleaner flow rate can enhance the filtration efficiency of SARS-CoV-2 laden droplets, it can also improve the convection in the indoor environment and potentially carry virus-laden droplets further and create a more scattered virus distribution in the patient room.
- The relative positions among the UV air cleaner, patient, and the main exhaust play a key role in the mitigation effectiveness of the exposure risks to airborne SARS-CoV-2 laden cough droplets.

The CFPD model employed in this study can provide guidance for the minimization of aerosol residence time as well as provide insight into mitigation strategies via non-pharmacological methods. It will be able to provide quantitative evidence on how to effectively prevent or even eliminate SARS-CoV-2 laden aerosols by introducing appropriate disinfection devices, optimizing the ventilation system, and modulating protocols of human interactions.

For future work, multiple UV air cleaners and room designs will be considered for a more generalized mitigation effectiveness evaluation. The CFPD modeling framework will be further



developed and serve as a rapid health risk assessment tool for operational directives when airborne infectious disease outbreaks occur in various indoor environments, such as classroom, office, restaurant, and auditorium.

ACKNOWLEDGMENTS

Funding for this project was provided by CoV-Eng (<https://coveng.org/>), a non-profit consortium of cross-disciplinary expertise established in response to COVID-19 pandemic. Funding for this project was also provided partially by the Southwest Center for Occupational and Environmental Health (SWCOEH), the Centers for Disease Control and Prevention (CDC) National Institute for Occupational Safety and Health (NIOSH) Education and Research Center (Grant # T42OH008421) at The University of Texas Health Science Center at Houston (UTHealth) School of Public Health (UTHealth) School of Public Health. The use of ANSYS software (Canonsburg, PA) as part of the ANSYS-CBBL academic partnership agreement is gratefully acknowledged (Dr. Thierry Marchal, Global Industry Director). Part of the numerical simulations was performed at the High-Performance Computing Center (HPCC), Oklahoma State University, supported in part through the National Science Foundation grant OAC-1531128.

REFERENCES

- Chen, X., Feng, Y., Zhong, W., Kleinstreuer, C. (2017). Numerical investigation of the interaction, transport and deposition of multicomponent droplets in a simple mouth-throat model. *J. Aerosol Sci.* 105, 108–127. <https://doi.org/10.1016/j.jaerosci.2016.12.001>
- Duguid, J.P. (1946). The size and the duration of air-carriage of respiratory droplets and droplet-nuclei. *Epidemiol. Infect.* 44, 471–479. <https://doi.org/10.1017/S0022172400019288>
- Feng, Y., Marchal, T., Sperry, T., Yi, H. (2020). Influence of wind and relative humidity on the social distancing effectiveness to prevent COVID-19 airborne transmission: A numerical study. *J. Aerosol Sci.* 147, 105585. <https://doi.org/10.1016/j.jaerosci.2020.105585>
- Feng, Y., Zhao, J., Chen, X., Lin, J. (2017). An in silico subject-variability study of upper airway morphological influence on the airflow regime in a tracheobronchial tree. *Bioengineering* 4, 90. <https://doi.org/10.3390/bioengineering4040090>
- Haghnegahdar, A., Feng, Y., Chen, X., Lin, J. (2018). Computational analysis of deposition and translocation of inhaled nicotine and acrolein in the human body with e-cigarette puffing topographies. *Aerosol Sci. Technol.* 52, 483–493. <https://doi.org/10.1080/02786826.2018.1447644>
- Haghnegahdar, A., Zhao, J., Feng, Y. (2019). Lung aerosol dynamics of airborne influenza A virus-laden droplets and the resultant immune system responses: An in silico study. *J. Aerosol Sci.* 134, 34–55. <https://doi.org/10.1016/j.jaerosci.2019.04.009>
- Kuga, K., Ito, K., Chen, W., Wang, P., Kumagai, K. (2020). A numerical investigation of the potential effects of e-cigarette smoking on local tissue dosimetry and the deterioration of indoor air quality. *Indoor Air* 30, 1018–1038 <https://doi.org/10.1111/ina.12666>
- Morawska, L., Tang, J.W., Bahnfleth, W., Bluyssen, P.M., Boerstra, A., Buonanno, G., Cao, J., Dancer, S., Floto, A., Franchimon, F. (2020). How can airborne transmission of COVID-19 indoors be minimised? *Environ. Int.* 142, 105832. <https://doi.org/10.1016/j.envint.2020.105832>
- National Institute for Occupational Safety and Health (NIOSH) (2015). Hierarchy of controls. <https://www.cdc.gov/niosh/topics/hierarchy/default.html>
- Thatiparti, D.S., Ghia, U., Mead, K.R. (2016). Assessing effectiveness of ceiling-ventilated mock airborne infection isolation room in preventing hospital-acquired influenza transmission to health care workers. *ASHRAE Trans.* 122, 35–46.
- Yang, L., Li, X., Yan, Y., Tu, J. (2018). Effects of cough-jet on airflow and contaminant transport in an airliner cabin section. *J. Comput. Multiphase Flows* 10, 72–82. <https://doi.org/10.1177/1757482X17746920>
- Zhao, J., Feng, Y., Bezerra, M., Wang, J., Sperry, T. (2019). Numerical simulation of welding fume lung dosimetry. *J. Aerosol Sci.* 135, 113–129. <https://doi.org/10.1016/j.jaerosci.2019.05.006>